CCFE
CULHAM CENTRE FOR FUSION ENERGY

UK Atomic Energy Authority

UKAEA-CCFE-PR(19)20

Sergei Gerasimov, P. Abreu, G Artaserse, M. Baruzzo, P. Buratti, I.S. Carvalho, I.H. Coffey, E. de la Luna, T.C. Hender, R.B. Henriques, R. Felton, U. Kruezi, P.J. Lomas, P. McCullen, M. Maslov, E. Matveeva, S. Moradi, L. Piron, F.G. Rimini, W. Schippers, G. Szepesi, M. Tsalas, L.E. Zakharov

Overview of disruptions with JET-ILW

Overview of disruptions with JET-ILW

Sergei Gerasimov, P. Abreu, G Artaserse, M. Baruzzo, P. Buratti, I.S. Carvalho, I.H. Coffey, E. de la Luna, T.C. Hender, R.B. Henriques, R. Felton, U. Kruezi, P.J. Lomas, P. McCullen, M. Maslov, E. Matveeva, S. Moradi, L. Piron, F.G. Rimini, W. Schippers, G. Szepesi, M. Tsalas, L.E. Zakharov

This is a preprint of a paper submitted for publication in Nuclear Fusion

Overview of disruptions with JET-ILW

S.N. Gerasimov[1], P. Abreu[2], G Artaserse[3], M. Baruzzo[4], P. Buratti[3], I.S. Carvalho[2], I.H. Coffey[1,5], E. de la Luna[6], T.C. Hender[1], R.B. Henriques[2], R. Felton[1], S. Jachmich[7,8], U. Kruezi[9], P.J. Lomas[1], P. McCullen[1], M. Maslov[1], E. Matveeva[10,11], S. Moradi[8], L. Piron[12], F.G. Rimini[1], W. Schippers[1], G. Szepesi[1], M. Tsalas[9], L.E. Zakharov[13,14,15] and JET Contributors[a]

EUROfusion Consortium, JET, Culham Science Centre, Abingdon, OX14 3DB, UK

[1] *CCFE, Culham Science Centre, Abingdon, Oxon, OX14 3DB, UK*
[2] *Instituto de Plasmas e Fusão Nuclear, Instituto Superior Técnico, Universidade de Lisboa, Lisboa, Portugal*
[3] *ENEA for EUROfusion, via E. Fermi 45, 00044 Frascati (Roma), Italy*
[4] *RFX, Corso Stati Uniti 4, Padova, Italy*
[5] *Astrophysics Research Centre, Queen's University, Belfast, BT7 1NN, UK*
[6] *Laboratorio Nacional de Fusión, CIEMAT, 28040 Madrid, Spain*
[7] *EUROfusion Programme Management Unit Culham, Culham Science Centre, Abingdon, UK*
[8] *Laboratory for Plasma Physics - LPP-ERM/KMS, Royal Military Academy, 1000-Brussels, Belgium*
[9] *ITER Organization, Route de Vinon, CS 90 046, 13067 Saint Paul Lez Durance, France*
[10] *Charles University, Faculty of Mathematics and Physics, Prague, Czech Republic*
[11] *Institute of Plasma Physics of the CAS, Prague, Czech Republic*
[12] *Università di Padova and Consorzio RFX, Corso Stati Uniti 4, 35127, Padova, Italy*
[13] *LiWFusion P.O. Box 2391, Princeton NJ 08543, USA*
[14] *Department of Physics, University of Helsinki, P.O. Box 43, FIN - 00014 University of Helsinki, Finland*
[15] *Department of Plasma Physics, National Research Nuclear University MEPhI, Moscow, 115409, Moscow, RF*

[a] *See the author list of "Overview of the JET preparation for Deuterium-Tritium Operation" by E. Joffrin et al. to be published in Nuclear Fusion Special issue: overview and summary reports from the 27th Fusion Energy Conference (Ahmedabad, India, 22-27 October 2018)*

E-mail: Sergei.Gerasimov@ukaea.uk

Abstract

The paper presents an analysis of disruptions occurring during JET-ILW plasma operations covering the period from the start of ILW (ITER-like wall) operation up to completion of JET operation in 2016. The total number of disruptions was 1951 including 466 with deliberately induced disruptions. The average rate of unintended disruptions is 16.1 %, which is significantly above the ITER target at 15 MA. The pre-disruptive plasma parameters are: plasma current I_p = (0.82 - 3.38) MA, toroidal field B_T = (0.98 - 3.4) T, safety factor q_{95} = (1.52 - 9.05). Massive gas injection (MGI) has been routinely used in protection mode both to terminate pulses when the plasma is at risk of disruption and to mitigate against disruption effects. The MGI was mainly triggered by the n = 1 locked mode amplitude exceeding a threshold or by the disruption itself;

either dI_p/dt or the toroidal loop voltage exceeding threshold values. For mitigation purposes, only the locked mode was used as a physics precursor to trigger the MGI prior to disruption. Long lasting locked modes (≥ 100 ms) do exist prior to disruption in 75% of cases. However, 10% of non-disruptive pulses have a locked mode which eventually vanished without disruption. The plasma current quench (CQ) may result in 3D equilibria, termed as asymmetrical disruptions, which are accompanied by sideways forces. Unmitigated VDEs (vertical displacement event) generally have significant plasma current toroidal asymmetries. MGI is a reliable tool to mitigate 3D effects and correspondingly sideways forces during the CQ. The vessel structure loads depend on the force impulse and force time behaviour including rotation. The toroidal rotation of 3D equilibria is of particular concern because of potential resonance with the natural frequencies of the vessel components in large tokamaks such as ITER. The amplitude-frequency interdependence is presented.

PACS numbers: 52.55.Fa

Submitted to*: Nuclear Fusion*

1. INTRODUCTION

The first non-disruptive tokamak pulse, also known as a magnetohydrodynamical (MHD) stable plasma, was obtained on the TM-2 tokamak in 1962 [1–3]. The TM-2 experiments manifested Shafranov's predictions for MHD stable plasmas [4]. The MHD mode structure during the pulse and prior to disruption was carefully investigated on the T3-A tokamak in 1970 [5]. It revealed a low m mode (m = 2) as a precursor to disruptions. During a major disruption a rapid change of the poloidal mode number from m = 2 to m = 3 was discovered on the T-6 tokamak in 1978 [6]. Later on disruption studies have been made in various tokamaks including JET [3,7–20]. Nevertheless, the occurrence and behaviour of disruptions remains poorly understood and so further studies have been made. This paper presents an analysis of disruptions occurring during JET-ILW (all metal wall with ITER-like Be/W composition [21]) plasma operations covering the period from 24/08/2011 (#80128, first ILW plasma pulse) up to 15/11/2016 (#92504).

In many tokamaks, massive gas injection (MGI) has become a popular tool to prevent machine damage during disruptions, particularly to eliminate melting of the Plasma Facing Component (PFC) and to mitigate disruption electromagnetic loads [18,19,22]. A disruption mitigation system (MGI and shattered pellet injection, SPI) is intended to be used on ITER [23,24]. On JET, MGI has been routinely used in protection mode, both to terminate pulses when the plasma is at risk of disruption and to mitigate against disruptions. Given that high stored energy plasma can damage beryllium tiles in the case of a disruption involving a VDE, the use of MGI is mandatory in JET for $I_p \geq 2.0$ MA or total plasma stored energy $W_{tot} \geq 5.0$ MJ. The MGI was mainly triggered by thresholds in the n = 1 locked mode amplitude or by the disruption itself, specifically by plasma current derivative (dI_p/dt) or by toroidal loop voltage thresholds. Hence, on JET only the n = 1 locked mode was treated as a physics precursor of disruptions for the purposes of triggering the MGI.

The plasma current quench (CQ) may result in 3D equilibria, termed as asymmetrical disruptions, which are accompanied by sideways forces [8,20,25–27]. The vessel structure loads

depend on the force impulse and force time behaviour including its rotation. The toroidal rotation of 3D equilibria is of particular concern because of potential resonance with the natural frequencies of the vessel components in large tokamaks such as ITER. The amplitude-frequency interdependence is important, since a simultaneous increase of amplitude and frequency would potentially create the most challenging load conditions. The JET-ILW disruption database which is used in this analysis is described in section 2. The composition of the different aspects of MGI usage is given in section 3. The update of the AVDE (Asymmetric Vertical Displacement Event) data, which extends the results presented in [8,20], is outlined in section 4. The $n = 1$ locked mode pre-disruptive behaviour is sketched in section 5. The results of the given disruption analyses are summarised in section 6.

2. DISRUPTION DATABASE AND STATISTICS

2.1. Disruption database

The JET-ILW upgrade was completed late in 2010 [21]. The first commissioning pulse #79856 was executed on 30/03/2011 with the first plasma pulse #80128 on 24/08/2011. The total number of JET shots with at least one powered poloidal field (PF) or toroidal field (TF) coil was 12649 in pulse range #79856 - #92504. In the present analysis, a shot is treated as a relevant plasma shot if the plasma current $|I_p| \geq 0.8$ MA for at least 0.25 s, Figure 1. Accordingly, the number of plasma pulses during JET-ILW operation was 9686, which corresponds to 77 % of the total number of shots. The magnetic diagnostic quantities, which are recorded at a 5 kHz sampling rate, have been used to identify the disruptive shots and define the time of disruption (T_{dis}). The quantities are two opposite octant average plasma current measurements (I_p), plasma current vertical centroid position (Z_p) and their derivatives, and toroidal loop voltages, which are measured at two poloidal locations on the inner wall of JET vessel, Figure 2. In this paper a left-hand coordinate system was chosen for disruption analyses, hence I_p is positive.

The loss of the poloidal magnetic flux due to the large MHD events causes the electromagnetic circuit of the plasma to respond with a positive spike in the plasma current. The induced negative current which flows in the vessel manifests itself as a large negative impulse in the toroidal full flux loops, V_{rru} and V_{rrl}, see Figure 2. The following disruption criteria have been used to build the disruption shot list:

(i) Fast drop of the plasma current, $-dI_p/dt > 20$ MA/s, for at least 0.25 ms, so it doesn't detect the fast I_p rise of the spike but only the drop;

(ii) Normalised average toroidal voltage $V_{rrAN} = (V_{rru} + V_{rrl})/2Ip < -13$ V/MA, Figure 3;

(iii) $|\Delta Z_p| > 0.225$ m (~a/4), where ΔZ_p is displacement respect of the steady-state prior to CQ, a is minor plasma radius, - VDE criteria.

The criteria (i) and (ii) indicate an ongoing disruption, while (iii) detects a loss of vertical control, i.e. the start of a VDE, which will result in a CQ. The pulse is treated as a disruption pulse if at least one of the (i) - (iii) criteria are met. The somewhat arbitrary choice of the criteria has been justified by manual analyses of the numerous disrupted pulses. It is worth mentioning that criteria (ii) and (iii) are not used in the real time (RT) JET disruption detection system. Instead, the product $V_{rru} \cdot V_{rrl}$ is used, which can detect a major disruption and also the start of VDE.

During #80128 - #92504 JET-ILW operation there were 1951 disruptive shots, including 466 with deliberately induced disruptions. 431 out of the 466 induced disruptions belong either to MGI (massive gas injection), or to VDE and EFCC (error field correction coil) experiments (i.e. intentional disruptions). The rest (35) of the induced disruptions were caused by various human errors or specific hardware/software tests or faults (however, such occurrences could equally be in the "un-intended" category). Hence the total number of unintended disruption pulses were 1951 - 466 = 1485 and the average disruption rate of unintended disruption was 1485/(9686-466) = 16.1% overall for JET-ILW pulses, Figure 4. The drop in Figure 4 in the range #83168 - #83795 belongs to a special experiment (“H-mode experiments for wall retention studies and long term sample analysis”), when 153 H-mode identical reliable pulses were executed [28].

However, 5 shots (3.3%) still disrupted, thus reflecting the lowest disruption rate during JET-ILW exploitation. It is thought that the plasma pollution by copper from NBI caused the disruptions in these cases, Figure 5 and Figure 6. The disruption rate significantly increases in the last group of pulses from #91960 to #92442, as shown in Figure 4. This can be attributed to exploration of operational space for high performance plasmas and optimisation in preparation for the upcoming JET DT campaigns going significantly outside the operational boundaries explored so far.

2.2. Disruption time

Disruption criteria (i) – (iii) are used to create the disruption shot list. Plasma pulses with multiple subsequent disruptions are very common. A special criterion is used to determine the major disruption in these cases:

(iv) If $|dI_p/dt| > 1$ MA/s between two sequential voltage spikes with $V_{rrAN} < -13$ V/MA,

then the disruption is defined to start at the first voltage spike. Should $|dI_p/dt| > 1$ MA/s not occur for the whole time between two sequential voltage spikes, then the disruption is defined to start at the second voltage spike. If $|dI_p/dt| > 1$ MA/s does not occur between any of the voltage spikes, then the last voltage spike with $I_p > 0.8$ MA defines the disruption; an example is shown in Figure 7. In this example, the plasma re-heats after the first major disruption event at ~13.3 s.

In the next stage the I_p, V_{rrAN} (for non-VDE) and ΔZ_p (for VDE) waveforms are analysed to extract a disruption time, T_{dis}. The T_{dis} calculated float value is rounded *down* to the nearest ms and that is what is recorded in database. Figure 8 illustrates T_{dis} calculation for a sharp plasma current spike and large loop voltage drop ($-dI_p/dt > 20$ MA/s and $V_{rrAN} < -13$ V/MA) disruption. In case of VDEs, ΔZ_p and its derivative are used to calculate T_{dis}, when $|\Delta Z_p| > 0.225$ m and $|dZ_p/dt| > 0.02$ m/ms, Figure 9.

2.3. Disruption classification

The pre-disruptive plasma current $I_p(T_{dis})$ = (0.82-3.38) MA and toroidal field the B_T (T_{dis}) = (0.98-3.4) T. Safety factor q_{95} = (1.53 - 9.1), plasma internal inductance l_i = (0.58 - 1.77), where dimensionless internal inductance $l_i \equiv l_i(3)$, normalized beta $\beta_N \leq 2.91$ (%·m·T/MA) [29], poloidal beta $\beta_p \leq 1.27$ and plasma configuration (X-point or limiter) were taken from 5 kHz EFIT [30,31] data which was available for 1420 out of 1485 unintended disruptive pulses. EFIT pre-disruptive plasma parameters are calculated as an average in the time window [T_{dis} -5 ms : T_{dis} - 1 ms]. The plasma has an X-point configuration prior to disruption for 720 pulses (~50%) out of 1420 pulses.

In majority of the unintended disruptive pulses (~96% from 1485 disruptions), the protection system detected an abnormal event such as a locked mode, impurity radiation, density limit, etc. prior to disruption. The majority of undetected unintended disruptions belong to hollow electron temperature collapse which is followed by disruption.

At disruption the Greenwald density limit fraction FGWL is in the (0.04-1.61) range, where FGWL is the line-averaged density divided by the Greenwald-density, $n_G = I_p/(\pi a^2)$ in (MA, m, 10^{20} m^{-3}) [32]. The line-average density is measured by the Thomson scattering diagnostics (HRTS and LIDAR) and mapped to a horizontal principal chord. The final available measurement of FGWL prior to disruption is presented in Figure 10. For normal operation we would expect a Greenwald fraction of 0.4 to 1.0. However, a failure of the gas fuelling system can result in very low Greenwald fractions, and conversely during current ramp-down the Greenwald fraction sometime rises up to 1.6.

Using three quantities, dI_p/dt, V_{rrAN} and ΔZ_p, the disruptions were sorted in four categories, specifically:

i. Fast I_p drop (> 20 MA/s) and large negative voltage spike (< -13 V/MA), 76.5 % of disruptions, Figure 11;
ii. Slow I_p drop and large negative toroidal voltage spike, 11.7 % of disruptions, Figure 12;

iii. Fast I_p drop and small negative toroidal voltage spike, 5.8 % of disruptions, Figure 13;

iv. VDE, 5.9 % of disruptions, Figure 9.

The empirical stability diagram, showing the l_i - q_{95} plane, has been used by various authors to present non-disruptive internal inductance and a boundary safety factor value [7,33,34]. The dimensionless internal inductance l_i and safety factor q_{95} are presented for all disruptions in the database in Figure 14. It is worth mentioning that the modern definition of internal inductance $l_i \equiv l_i(3)$ differs from reference [7,33,34], hence direct quantity comparison is not straightforward. The category (i) disruption has an extended cloud of points, while category (iii) disruptions are characterised by flat current profile and moderate safety factor.

The physical reason for some separation of (i) – (iii) categories is an outstanding issue, which will be the subject of a future study.

3. MGI USAGE

3.1. MGI triggering statistic

MGI has been routinely used in protection mode both to terminate pulses when the plasma is at risk of disruption, and to mitigate the potentially damaging impact of disruptions on the vessel and the PFC [18,35–37]. During JET-ILW plasma operations (from #80128 up to #92504), in total 896 shots were ended by MGI, using typically an optimum gas mixture of 90% D2 + 10% Ar. The amount of injected gas varies from 1.6 *bar·l* (6.8E+22 D2 atoms + 3.8E+21 Ar atoms) to 10.7 *bar·l* for DMV3 (Disruption Mitigation Valve #3, named "Top,S" in [37]) and from 1.9 *bar·l* to 26.3 *bar·l* for DMV2 (Disruption Mitigation Valve #2, named "Midpl" in [37]). It is worth mentioning that the quantity of injected atoms at 1.6 *bar·l* exceeds the total number of electrons in pre-disruptive plasma by approximately a factor 2.

In the majority of the mitigated disruptions, the MGI was triggered by a $n = 1$ locked mode threshold (523 shots) or by the disruption itself, specifically by dI_p/dt (207 shots) or by the

toroidal loop voltage (145 shots). There are 21 exceptional cases when a MGI was triggered by other causes including pick up of an $n = 2$ mode oscillation by plasma vertical control system (14 shots), and other various tests and faults. Moreover, 249 disruption shots were dedicated for MGI experiments.

The High Voltage (HV) JET system, which includes the auxiliary heating (NBI, ICRH, LH) and some diagnostics (Li-beam, NPA, VUV spectroscopy, etc.) have to be in a safe state when large gas quantities arrive in the vessel, hence the HV systems impose a delay before the MGI is fired. The initial MGI usage set up conservative a HV delay up to 60 ms; however later the requested HV delay was reduced to as low as ~10 ms, Figure 15. The decrease in delay time is due to the implementation of a check on whether the NBI or RF power supplies have turned off.

3.2. Effect of MGI on CQ duration

The MGI increases plasma radiation, which has the effect of reducing both thermal loads and CQ duration, which additionally helps to reduce thermal loads on PFC [19]. The CQ duration is described by $\tau_{80/20}$, which is the time linearly extrapolated from the time taken to quench from 80% to 20% of I_{dis}. The recommended value of $\tau_{80/20}$ for JET should be in the region 10 – 27.5 ms, which is a somewhat arbitrary choice. However, the low threshold given by force loads on the machine [38] and the upper threshold is justified by minimisation of thermal loads.

The CQ duration strongly depends on the injected gas amount and pre-disruptive plasma current, Figure 16 and Figure 17. Moreover, two main MGI systems, DMV2 and DMV3 (DMV1 was replaced by SPI during the 2016-18 shutdown) have different geometrical parameters [37]. To deliver the same amount of gas DMV2 must operate at ~ 3 time higher pressure than DMV3. Thus, the efficiency of DMV2, in terms of $\tau_{80/20,}$ is a factor of ~2 higher than DMV3, Figure 16. The CQ duration rises with pre-disruptive plasma current, which may reflect the dependence of $\tau_{80/20}$ from I_p magnetic energy to be dissipate.

For MGI mitigated shots, the distribution of the fraction of occurrences is shifted to low CQ time and is much narrower in comparison with non-mitigated disruptions, Figure 18; this is consistent with modelling where MGI boosts MHD instabilities, which enhance the penetration of the gas into the plasma, [39,40]. On JET, when MGI is fired in "healthy", pre-disruptive and post-disruptive plasma, there are small differences in the CQ duration; it is surprising that the fraction of occurrences shifts slightly towards lower CQ times for MGI experiments, when the gas is fired mainly into healthy plasmas, Figure 19.

3.3. Impact MGI on vessel vertical force

The electro-magnetic (EM) loads arise during the CQ when currents were driven in machine conductive structures [8,19,20,26]. Due to the EM loads, the JET vessel experiences oscillatory deformations, while vessel vertical reaction forces (F_v) are measured. Figure 20 shows three shots: a VDE, an MGI terminated pulse and a central disruption followed by large plasma displacement during the CQ. There are minor differences in F_v, in general, for MGI mitigated disruptions: vertical forces are below non-mitigated disruptions, particularly non-mitigated VDEs, Figure 21. However, there are several non-MGI cases with the force lower than with MGI for the same plasma current. A result of scatter could be due to specific uncontrollable behaviour of plasma vertical position control system during the CQ or other effects, e.g variation in plasma shape. A (33-40)% reduction in F_v due to MGI [37] was obtained for specific identical pulses.

4. ASYMMETRIC VDE

The plasma CQ may result in 3D equilibria, termed "asymmetrical disruptions", which are accompanied by sideways forces [8,20]. At least 3 toroidally distributed measurements of I_p are needed for analyses [8]. The 5 kHz magnetics data from four toroidally orthogonal locations has been recorded for 95% of the disruptive pulses [8].

Unmitigated VDEs generally have significant plasma current toroidal asymmetries $A = \int A_p^{asym}\, dt$, where $A_p^{asym} = I_p^{asym} / \left| I_p^{dis} \right|$, $I_p^{asym} = \sqrt{\left(I_{p7} - I_{p3}\right)^2 + \left(I_{p5} - I_{p1}\right)^2}$ with I_{p1} = octant 1 plasma current measurement etc. Figure 22 . The development of the toroidal asymmetry is preceded by the drop to unity of q_{95}, see Figure 22d and [8,20]. However, MGI is a reliable tool to mitigate 3D non axisymmetric effects and correspondingly sideways forces [41] during the CQ, Figure 23. To achieve the mitigation, the MGI, termed "efficient" on Figure 23, with proper pressure and gas composition must be fired in the early phase of the VDE [8]. Unmitigated disruptions also have large plasma current asymmetries, presumably because there is no proper plasma vertical position control during CQ, though the plasma vertical position control system is still active, but can't provide adequate reaction. On Figure 23, the large scatter in the blue points which fill the space between the green MGI points and the red VDE (without mitigation) reflects the plasma VDE-like behaviour during the CQ after "central" major disruption.

The vessel structure loads depend on the force impulse and force time behaviour or rotation. The toroidal rotation of 3D equilibria is of particular concern because of potential resonance with the natural frequencies of the vessel components in large tokamaks such as ITER [42]. The I_p asymmetry amplitude-frequency calculation procedure is illustrated by Figure 24. For each disruptive shot, the maximum and minimum toroidal phases (calculated from sine, ~ $(I_{p7} - I_{p3})$, and cosines, ~ $(I_{p5} - I_{p1})$, components) of an I_p asymmetry define the number of turns, N_{turn}; the corresponding time window, Δt, is defined when A_p^{asym} > threshold. The rotational frequency is calculated as $f = N_{turn}/\Delta t$. The rotational frequency, f is plotted against an average during Δt time window of the I_p asymmetry, $\langle I_p^{asym} \rangle = \langle A_p^{asym} \rangle I_p^{dis}$ in Figure 25.

The amplitude-frequency interdependence is important, since a simultaneous increase of amplitude and frequency would potentially create the most challenging load conditions. However fortunately, the amplitude envelope of the plasma current asymmetries decreases with increasing frequency, Figure 25.

The distribution is not symmetric around zero frequency. The rotation is mainly observed in the electron drift direction, a positive value indicates anticlockwise rotation opposite to the negative plasma current and negative toroidal field [8]. Understanding the origin and direction of I_p asymmetry rotation is still an outstanding issue.

5. LOCKED MODE AND DISRUPTION

The n = 1 locked mode amplitude and phase are obtained from saddle loops allocated in 4 octants which are shifted by 90^o toroidally to each other [8]. In each octant two saddles near the middle plane of the machine on the low field side are used for the calculation of the locked mode amplitude, *Loca*, and its normalised equivalent $LocaN = Loca/I_p$.

In general, disruptions at JET have a locked or slowly rotating mode precursor [16,34,43]. The MGI was mainly triggered by the n = 1 locked mode amplitude exceeding a threshold or by the disruption itself, specifically either dI_p/dt or the toroidal loop voltage exceeding threshold values. For mitigation purposes, only the locked mode was treated as a precursor (i.e. the cause of disruptions). In these cases, the MGI was triggered by a locked mode threshold, in either *Loca* or *LocaN*. On JET, the common threshold to trigger the DMV is 0.2 mT/MA. The locked mode amplitude presented in Figure 26 was cleaned from a parasitic offset, while real time *LocaN* signal usually has 0.1 mT/MA offset.

The subset of 913 natural disruptions (in the range of I_p^{dis}= (0.84 – 3.14) MA) , which were not affected by special dedicated experiments or MGI protection (i.e. the subset includes shots when MGI was triggered by locked mode amplitude thresholds, but does not include shots when MGI was triggered by dI_p/dt or loop voltage thresholds), was used for analysis of pre-disruptive plasma behaviour. The threshold in normalised locked mode amplitude of 0.1 mT/MA was taken on as an indicator of locked mode. A time ΔT_{01b} was defined as the time between this threshold being exceeded for the final time before disruption time (T_{dis}), Figure 26. The ΔT_{01b} quantity,

presented in Figure 27 shows that long lasting locked modes (≥ 100 ms) do exist prior to disruption in 70% of disruptions with locked mode precursor. Locked modes with $\Delta T_{01b} \geq 10$ ms occur prior to disruption in the majority of cases (94%). The locked mode exists prior to natural disruptions in 98% cases. Only 5% disruptions out of 913 disrupted with locked mode precursor duration $\Delta T_{01b} \leq 5$ ms or without a locked mode precursor. Though, 10% of non-disruptive pulses have a locked mode with amplitude greater than 0.1 mT/MA, which eventually vanished without disruption. The presented data could suggest that the locked mode is not a primary causation of disruptions but is a good indicator of unhealthy plasma condition. Further deep analyses are needed to reveal the role of the locked mode in pre-disruptive plasma.

6. SUMMARY

JET-ILW data are presented for machine operation from 2011 (#80128) until 2016 (#92504). During this period, 1951 disruptions occurred, including 466 deliberate disruption experiments. Thus, the average disruption rate of unintended disruptions is 16.1 %, which is significantly above the ITER target for full plasma current operation.

Three quantities, dI_p/dt, V_{rrAN} and ΔZ_p, have been used to sort disruptions into four categories. The pre-disruptive plasma equilibrium parameters create a cloud on the l_i-q_{95} stability diagram. Three separate categories (apart from VDEs) can be seen on the l_i-q_{95} stability diagram, which may help better understand the nature of disruptions.

MGI has routinely been used to protect the PFC in the metal wall. It is also an effective tool to eliminate plasma current asymmetries (i.e. sideways forces).

The toroidal rotation of 3D equilibria is of particular concern due to the potential resonance with the natural frequencies of the vessel components in large tokamaks such as ITER. In JET, the

amplitude envelope of the plasma current asymmetries decreases as the magnitude of the observed rotation frequency increases. This is a positive result for large tokamaks.

The locked mode occurs prior to the majority of natural disruption. However, the locked mode usually exists for a long time before the disruption occurs, which could suggest it is not a primary causation of disruptions but is a good indicator of unhealthy plasma condition.

The presented JET-ILW disruption data provide an opportunity for the calibration of the numerical models.

ACKNOWLEDGEMENTS

This work has been carried out within the framework of the EUROfusion Consortium and has received funding from the Euratom research and training programme 2014-2018 and 2019-2020 under grant agreement No 633053 and from the RCUK Energy Programme [EP/P012450/1]. To obtain further information on the data and models underlying this paper please contact PublicationsManager@ukaea.uk. The views and opinions expressed herein do not necessarily reflect those of the European Commission. Partially the work was supported by Grant 14.Y26.31.0008 from Ministry of Education and Science of Russian Federation. The authors are grateful to E. Joffrin for fruitful discussions during the course of this work.

REFERENCES

[1] Gorbunov E P and Razumova K A 1964 Effect of a strong magnetic field on the magnetohydrodynamic stability of a plasma and the confinement of charged particles in the `Tokamak' machine *J. Nucl. Energy. Part C, Plasma Physics, Accel. Thermonucl. Res.* **6** 515–25

[2] Mirnov S V. 2016 V. D. Shafranov and Tokamaks *J. Plasma Phys.* **82** 1–20

[3] Mirnov S V 2019 Tokamak evolution and view to future *Nucl. Fusion* **59** 015001

[4] Shafranov V D 1959 On the stability of a plasma column in the presence of the longitudinal magnetic field and the conducting casing *Plasma Phys. and the Prob. of Contr. Therm. React. Vol.1 -Translated from Atomnaya Énergiya Vol. 5 pp.38-41 1956* (Pergamon Press) pp 207–13

[5] Mirnov S V and Semenov I B 1971 Investigation of the instabilities of the plasma string in the Tokamak-3 system by means of a correlation method *Sov. At. Energy - Transl. from At. Énergiya, Vol.30, No.1, pp.20–27, January, 1971* **30** 22–9

[6] Soediono B 1989 No Title No Title *J. Chem. Inf. Model.* **53** 160

[7] Wesson J A, Gill R D, Hugon M, Schüller F C, Snipes J A, Ward D J, Bartlett D V, Campbell D J, Duperrex P A, Edwards A W, Granetz R S, Gottardi N A O, Hender T C, Lazzaro E, Lomas P J, Cardozo N L, Mast K F, Nave M F F, Salmon N A, Smeulders P, Thomas P R, Tubbing B J D, Turner M F and Weller A 1989 Disruptions in JET *Nucl. Fusion* **29** 641

[8] Gerasimov S N, Abreu P, Baruzzo M, Drozdov V, Dvornova A, Havlicek J, Hender T C, Hronova O, Kruezi U, Li X, Markovič T, Pánek R, Rubinacci G, Tsalas M, Ventre S, Villone F and Zakharov L E 2015 JET and COMPASS asymmetrical disruptions *Nucl. Fusion* **55** 113006

[9] Sweeney R, Choi W, Austin M, Brookman M, Izzo V, Knolker M, La Haye R J,

Leonard A, Strait E and Volpe F A 2018 Relationship between locked modes and thermal quenches in DIII-D *Nucl. Fusion* **58**

[10] T C Hender, G Arnoux, P de Vries, S Gerasimov, A Huber, M F Johnson and R Koslowski, M Lehnen, A Loarte, J.R. Martín-Solís V R 2010 JET disruption studies in support of ITER *Proc. 23rd Int. Conf. Fusion Energy 2010 (Daejeon, Korea, 11–16 Oct. 2010) (Vienna IAEA)* **EXS/10-3**

[11] Fougeres C, Joffrin E, Nardon E, Alessi E, Buratti P, Ficker A, Rfx C and Uniti C S 2018 Magnetic fluctuations during the thermal and current quench of mitigated disruptions and comparison with 3D non-linear MHD predictions *45th Eur. Phys. Soc. Conf. Plasma Phys. (Prague, Czech Republic, 2 - 6 July 2018)* **Vol. 42A** O3.106

[12] Schuller F C 1995 Disruptions in tokamaks *Plasma Phys. Control. Fusion* **37**

[13] Riccardo V 2003 Disruptions and disruption mitigation *Plasma Phys. Control. fusion* **45** A269–84

[14] de Vries P C, Johnson M F and Segui I 2009 Statistical analysis of disruptions in JET *Nucl. Fusion* **49** 055011

[15] Riccardo V, Arnoux G, Cahyna P, Hender T C, Huber A, Jachmich S, Kiptily V, Koslowski R, Krlin L, Lehnen M, Loarte A, Nardon E, Paprok R and Tskhakaya D 2010 JET disruption studies in support of ITER *Plasma Phys. Control. Fusion* **52** 124018

[16] de Vries P C, Johnson M F, Alper B, Buratti P, Hender T C, Koslowski H R and Riccardo V 2011 Survey of disruption causes at JET *Nucl. Fusion* **51** 053018

[17] Lehnen M, Gerasimov S N, Jachmich S, Koslowski H R, Kruezi U, Matthews G F, Mlynar J, Reux C and Vries P C De 2015 Radiation asymmetries during the thermal quench of massive gas injection disruptions in JET *Nucl. Fusion* **55** 123027

[18] Lehnen M, Alonso A, Arnoux G, Baumgarten N, Bozhenkov S A, Brezinsek S, Brix M, Eich T, Gerasimov S N, Huber A, Jachmich S, Kruezi U, Morgan P D, Plyusnin V V., Reux C, Riccardo V, Sergienko G and Stamp M F 2011 Disruption mitigation by

massive gas injection in JET *Nucl. Fusion* **51** 123010

[19] Lehnen M, Arnoux G, Brezinsek S, Flanagan J, Gerasimov S N, Hartmann N, Hender T C, Huber A, Jachmich S, Kiptily V, Kruezi U, Matthews G F, Morris J, Plyusnin V V, Reux C, Riccardo V, Sieglin B and De Vries P C 2013 Impact and mitigation of disruptions with the ITER-like wall in JET *Nucl. Fusion* **53** 93007–13

[20] Gerasimov S N, Hender T C, Morris J, Riccardo V and Zakharov L E 2014 Plasma current asymmetries during disruptions in JET *Nucl. Fusion* **54** 073009

[21] Riccardo V, Lomas P, Matthews G F, Nunes I, Thompson V and Villedieu E 2013 Design, manufacture and initial operation of the beryllium components of the JET ITER-like wall *Fusion Eng. Des.* **88** 585–9

[22] Pautasso G, Bernert M, Dibon M, Duval B, Dux R, Fable E, Fuchs J C, Conway G D, Giannone L, Gude A, Herrmann A, Hoelzl M, McCarthy P J, Mlynek A, Maraschek M, Nardon E, Papp G, Potzel S, Rapson C, Sieglin B, Suttrop W and Treutterer W 2017 Disruption mitigation by injection of small quantities of noble gas in ASDEX Upgrade *Plasma Phys. Control. Fusion* **59**

[23] Lehnen M, Aleynikova K, Aleynikov P B, Campbell D J, Drewelow P, Eidietis N W, Gasparyan Y, Granetz R S, Gribov Y, Hartmann N, Hollmann E M, Izzo V A, Jachmich S, Kim S H, Kočan M, Koslowski H R, Kovalenko D, Kruezi U, Loarte A, Maruyama S, Matthews G F, Parks P B, Pautasso G, Pitts R A, Reux C, Riccardo V, Roccella R, Snipes J A, Thornton A J and De Vries P C 2015 Disruptions in ITER and strategies for their control and mitigation *J. Nucl. Mater.* **463** 39–48

[24] Hollmann E M, Aleynikov P B, Fülöp T, Humphreys D A, Izzo V A, Lehnen M, Lukash V E, Papp G, Pautasso G, Saint-Laurent F and Snipes J A 2015 Status of research toward the ITER disruption mitigation system *Phys. Plasmas* **22**

[25] P. Noll, P. Andrew, M. Buzio, R. , Litunovsky, T. Rainmondi, V. Ricardo M V 1996 Present understanding of electromagnetic behaviour during disruptions at JET *Proc.*

19th Symp. Fusion Technol. (Lisbon, Port. 16–20 Sept. 1996)

[26] Riccardo V, Noll P and Walker S 2000 Forces between plasma, vessel and TF coils during AVDEs at JET *Nucl. Fusion* **40** 1805–10

[27] Riccardo V, Walker S and Noll P 2000 Parametric analysis of asymmetric vertical displacement events at JET *Plasma Phys. Control. Fusion* **42** 29–40

[28] Heinola K, Widdowson A, Likonen J, Alves E, Barradas N, Brezinsek S, Catarino N, Coad P, Koivuranta S, Krat S, Matthews G F, Mayer M, Petersson P and Contributors J E T 2016 Long-term fuel retention in JET ITER- like wall *Phys. Scr.* **T167** 1–7

[29] F Troyon, R Gruber, H Saurenmann S S and S S 1984 MHD-Limits to Plasma Confinement *Plasma Phys. Control. Fusion* **26** 209

[30] L.L. Lao, H. St. John, R.D. Stambaugh, A.G. Kellman, W. Pfeiffer 1985 Reconstruction of current profile parameters and plasma shapes in tokamaks *Nucl. Fusion* **25** 1611

[31] O'Brien D ., Lao L ., Solano E ., Garribba M, Taylor T ., Cordey J . and Ellis J . 1992 Equilibrium analysis of iron core tokamaks using a full domain method *Nucl. Fusion* **32** 1351–60

[32] Greenwald M 2002 Density limits in toroidal plasmas *Plasma Phys. Control fusion* **44** 1–55

[33] Cheng C Z, Furth H P and Boozer A H 1987 MHD stable regime of the Tokamak *Plasma Phys. Control. Fusion* **29** 351–66

[34] Snipes J A, Campbell D J, Hugon M, Lomas P J, Nave M F F, Haynes P S, Hender T C, Lopes Cardozo N J and Schüller F C 1988 Large amplitude quasi-stationary MHD modes in JET *Nucl. Fusion* **28** 1085–97

[35] E. Joffrin, E. Alessi, M. Baruzzo, P. C. de Vries, P. Drewelow, A. Fil, S. Gerasimov, T.C. Hender, S. Jachmich, U. Kruezi, M. Lehnen, A. Murari, R. Moreno, B. NKonga, E. Nardon, I. Nunes, R. Paccagnella, A. Pau, C. Reux, V. Riccardo, R. Roccella C S 2016 Disruption study advances in the JET metallic wall *Proc. 26th IAEA Fusion Energy*

Conf. (Kyoto, Japan, 17-22 Oct. 2016) EX-9.1

[36] de Vries P C, Arnoux G, Huber A, Flanagan J, Lehnen M, Riccardo V, Reux C, Jachmich S, Lowry C, Calabro G, Frigione D, Tsalas M, Hartmann N, Brezinsek S, Clever M, Douai D, Groth M, Hender T C, Hodille E, Joffrin E, Kruezi U, Matthews G F, Morris J, Neu R, Philipps V, Sergienko G and Sertoli M 2012 The impact of the ITER-like wall at JET on disruptions *Plasma Phys. Control. Fusion* **54** 124032

[37] S. Jachmich, P. Drewelow, S. Gerasimov, U. Kruezi, M. Lehnen, C. Reux, V. Riccardo, I. Carvalho, A. Pau, M. Imsirek E J 2016 Disruption mitigation at JET using massive gas injection *43rd Eur. Phys. Soc. Conf. Plasma Physics, EPS 2016* 8–11

[38] V. Riccardo, P. Andrew, A. Kaye P N 2002 Disruption design criteria for JET in-vessel components *Proc. 19th IEEE/IPSS Symp. Fusion Eng. 19th SOFE* 384–7

[39] Nardon E, Fil A, Hoelzl M and Huijsmans G 2017 Progress in understanding disruptions triggered by massive gas injection via 3D non-linear MHD modelling with JOREK *Plasma Phys. Control. Fusion* **59** 014006

[40] Izzo V A 2013 Impurity mixing and radiation asymmetry in massive gas injection simulations of DIII-D *Phys. Plasmas* **20**

[41] Gerasimov S N and T.C. Hender, M.F. Johnson L E Z 2010 Scaling JET Disruption Sideways Forces to ITER *37th Eur. Phys. Soc. Conf. Plasma Phys. (Dublin, Ireland, 21–25 June 2010)* **Vol. 34A** P4.121

[42] Myers C E, Eidietis N W, Gerasimov S N, Gerhardt S P, Granetz R S, Hender T C and Pautasso G 2018 A multi-machine scaling of halo current rotation *Nucl. Fusion* **58** 016050

[43] M.F.F. Nave, J. A. Wesson 1990 Mode locking in tokamaks *Nucl. Fusion* **30** 2575–83

Figures

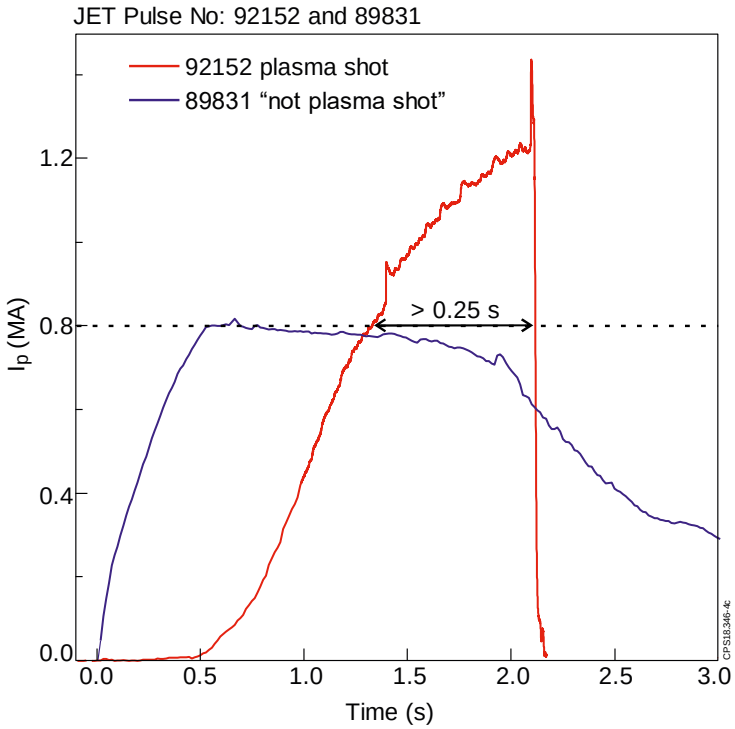

Figure 1. Only shots with plasma current $|I_p| \geq 0.8$ MA for at least 0.25 s were used for disruption database.

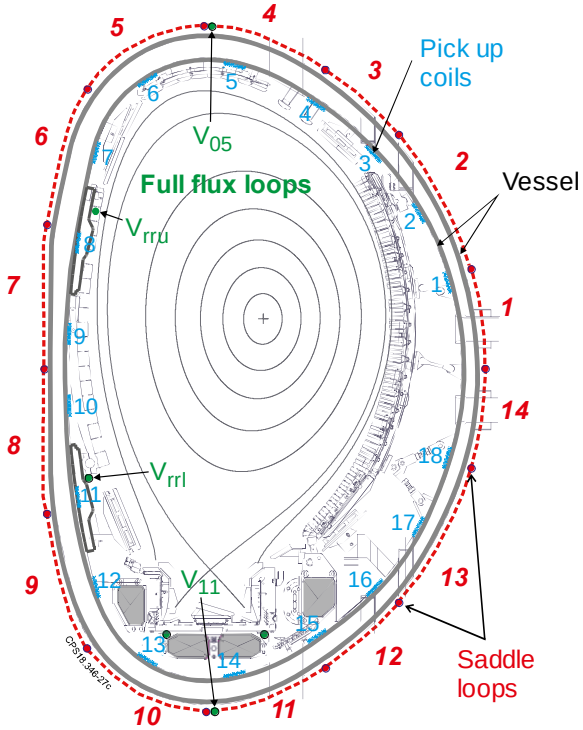

Figure 2. JET magnetic diagnostics used to identify the disruption shots: in-vessel pick up coils for plasma current, pick up coils and ex-vessel saddle loops for plasma current vertical centroid position and toroidal loop voltages.

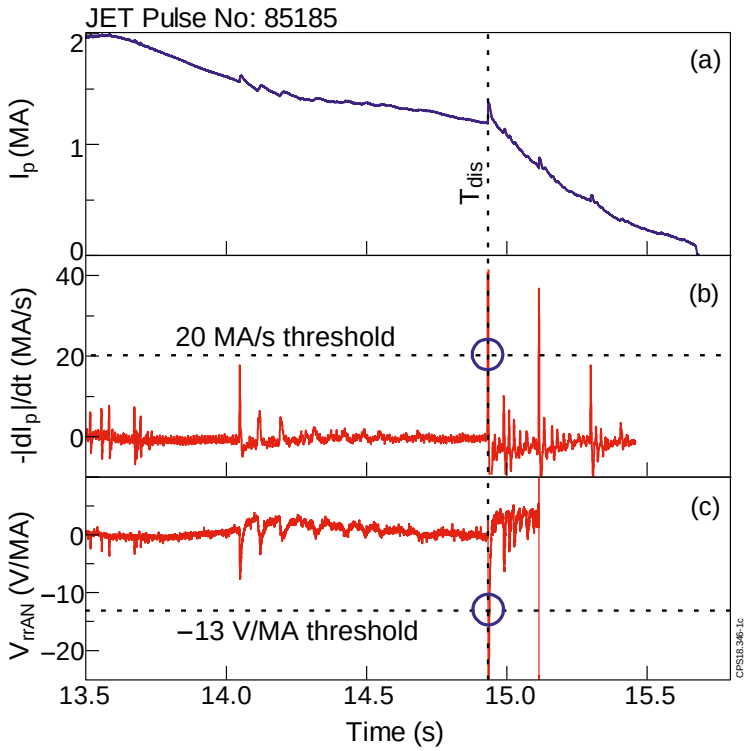

Figure 3. Major disruption must satisfy at least one criterion, $-dI_p/dt > 20$ MA/s or $V_{rrAN} < -13$ V/MA: (a) plasma current, (b) plasma current derivative (c) normalised toroidal voltage.

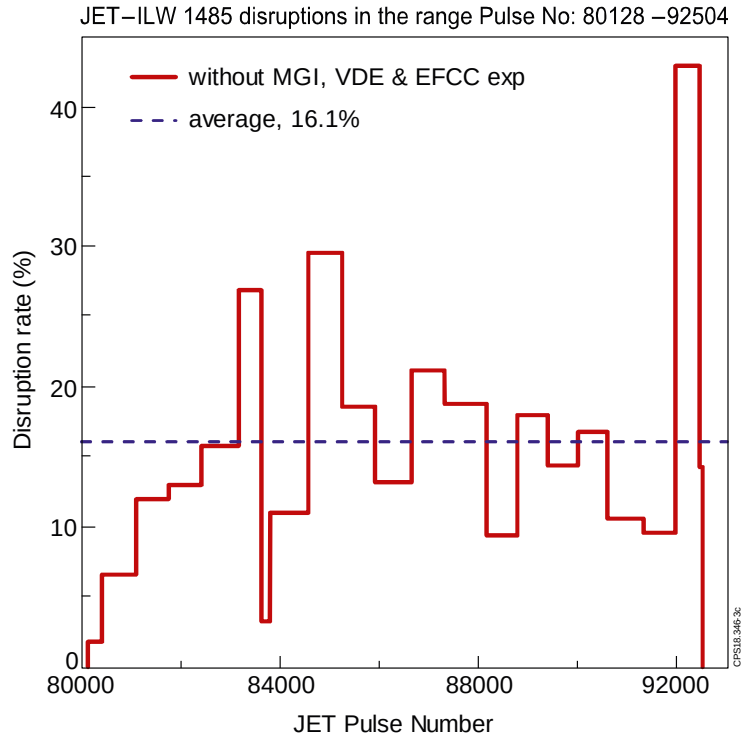

Figure 4. Disruption rate during whole JET-ILW campaign.

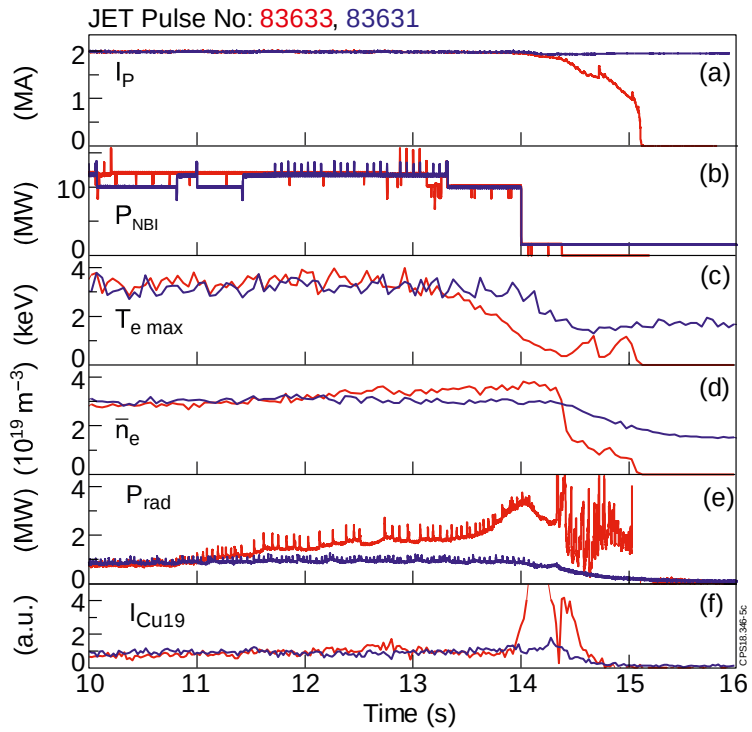

Figure 5**.** The waveforms of the EX-1.2.5 pulses: (a) plasma current, (b) NBI power, (c) maximum electron temperature, (d) average electron liner density, (e) total bolometer power, (f) Cu19 line (273.36 Å) emission intensity.

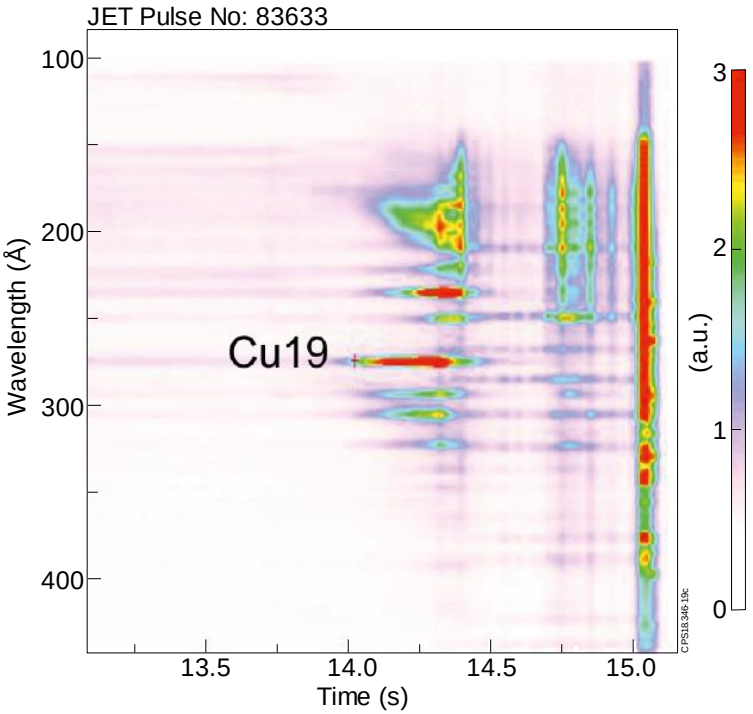

Figure 6. Impurity emission prior to disruption from a VUV spectrometer.

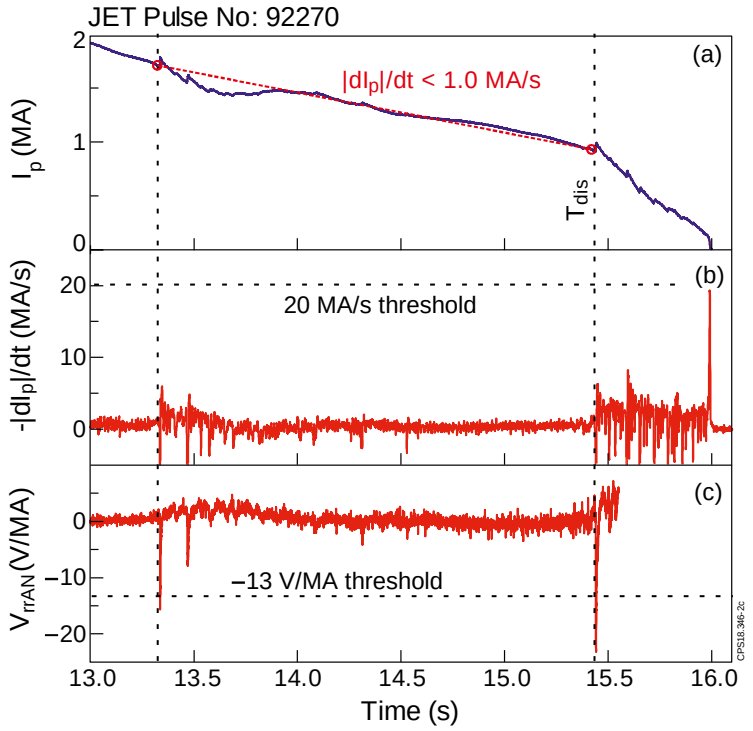

Figure 7. Illustration of criterion (iii) usage: (a) plasma current, (b) plasma current derivative (c) normalised toroidal voltage. In this case the disruption is defined to start at 15.440 s because of a slow I_p drop after the first major disruption at 13.336 s.

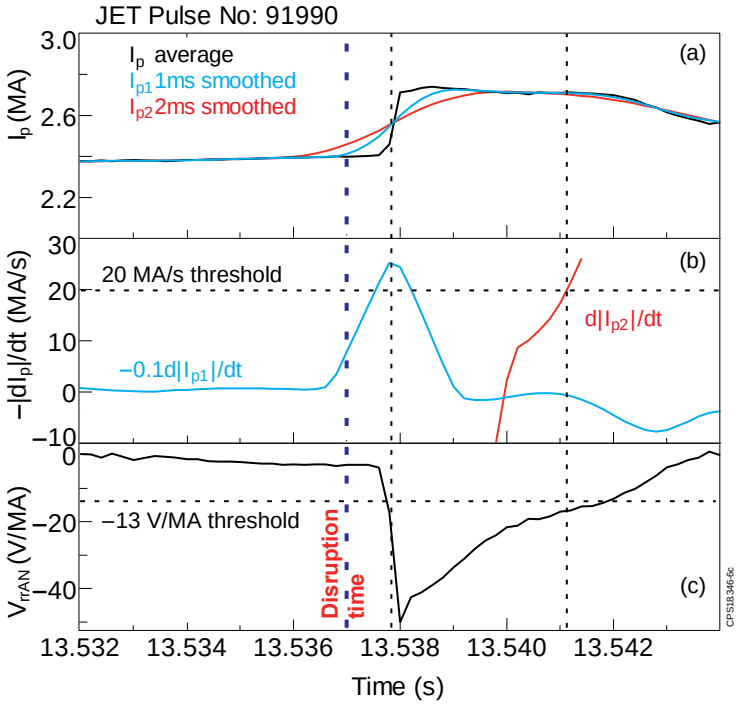

Figure 8. Illustration of T_{dis} calculation: (a) plasma currents, (b) plasma current derivatives, (c) normalised toroidal voltage. $d|I_{p2}|/dt$ has a delay because it reflects the I_p drop during plasma current spike.

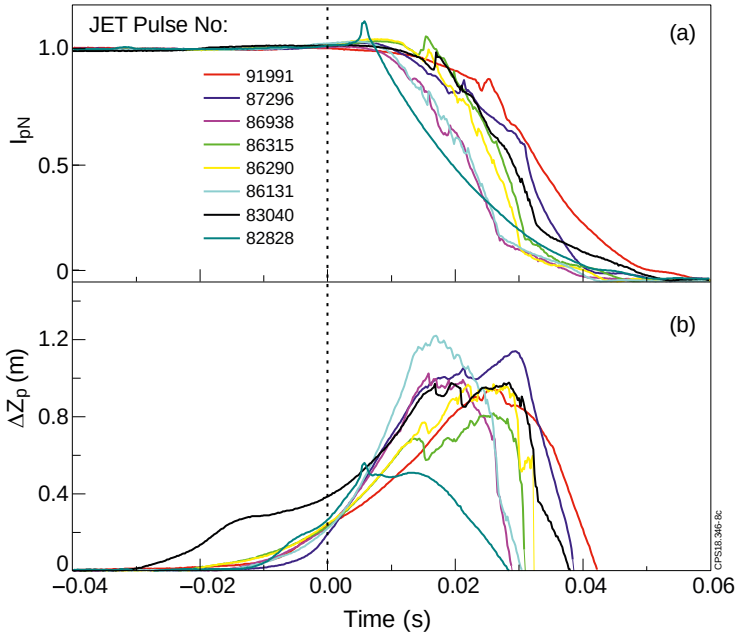

Figure 9. Illustration of T_{dis} calculation for VDE: (a) normalised plasma currents, (b) normalised plasma displacement. The time axis is zeroed to T_{dis}.

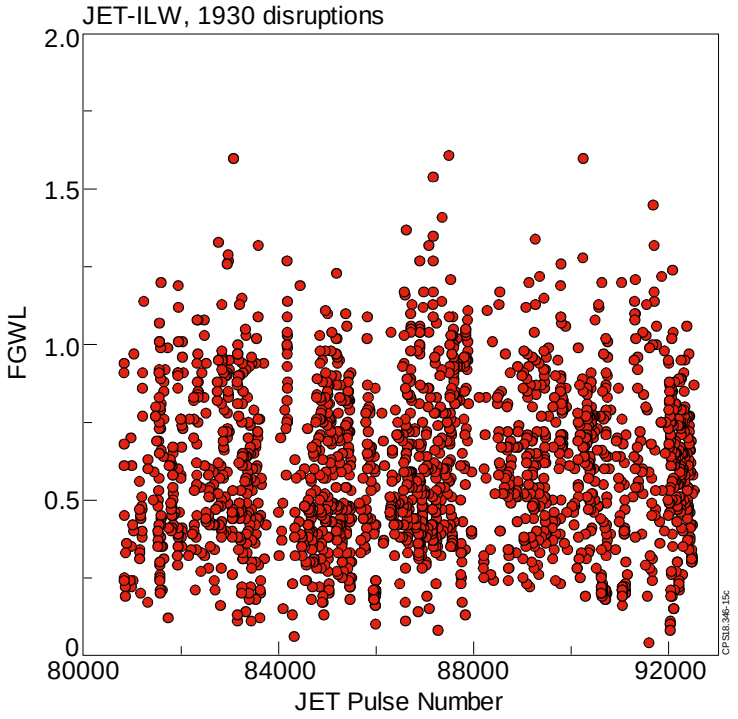

Figure 10. JET plasma pre-disruptive fraction of Greenwald density limit varies significantly.

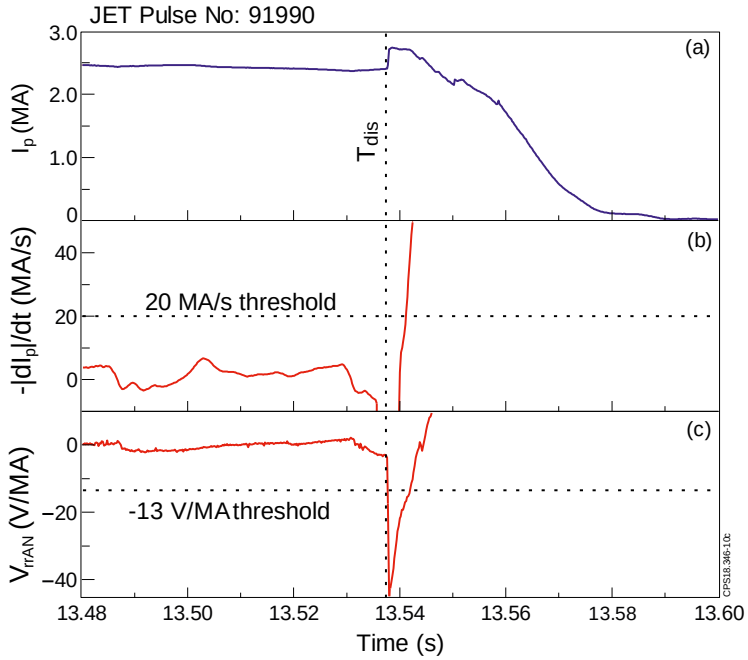

Figure 11. An example of disruption with fast I_p drop and large negative voltage spike: (a) plasma current, (b) plasma current derivative, (c) normalised toroidal voltage.

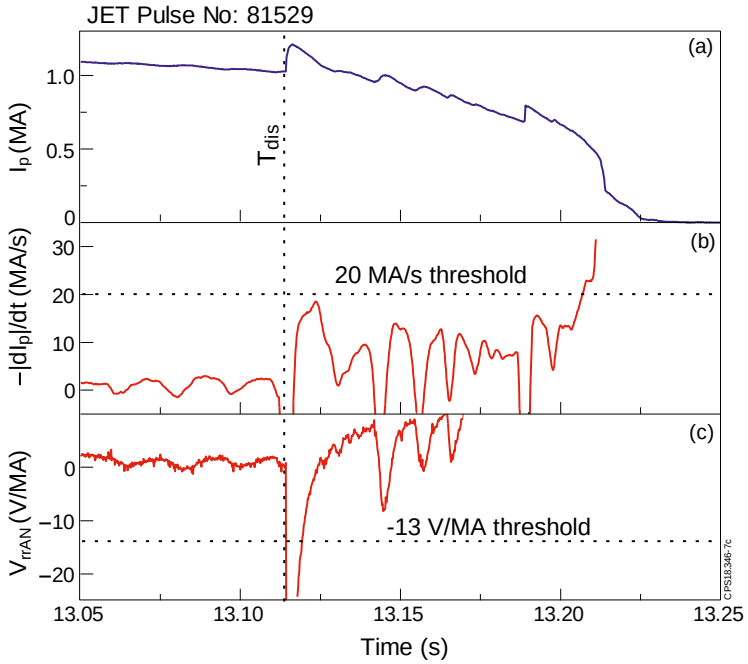

Figure 12. An example of disruption with slow I_p drop and large negative voltage spike: (a) plasma current, (b) plasma current derivative, (c) normalised toroidal voltage.

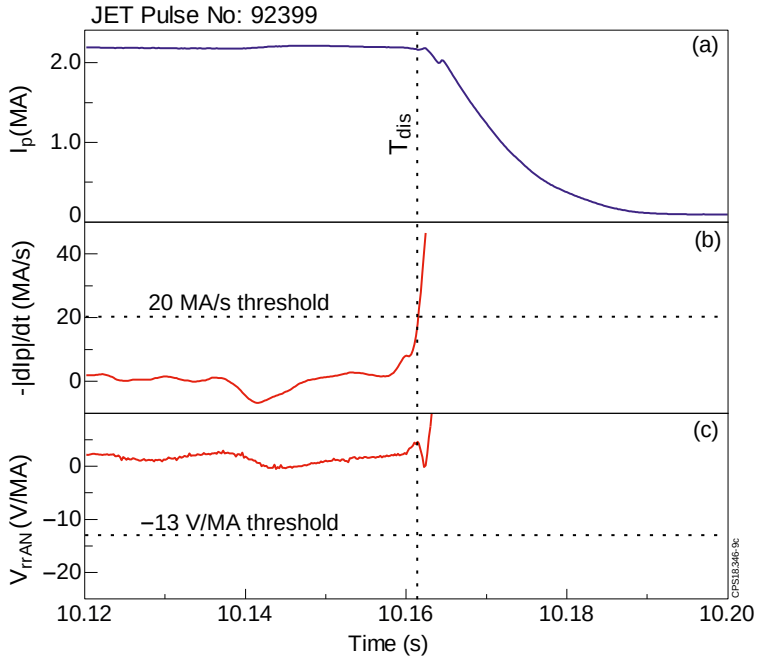

Figure 13. An example of disruption with fast I_p drop and small negative voltage spike: (a) plasma current, (b) plasma current derivative, (c) normalised toroidal voltage.

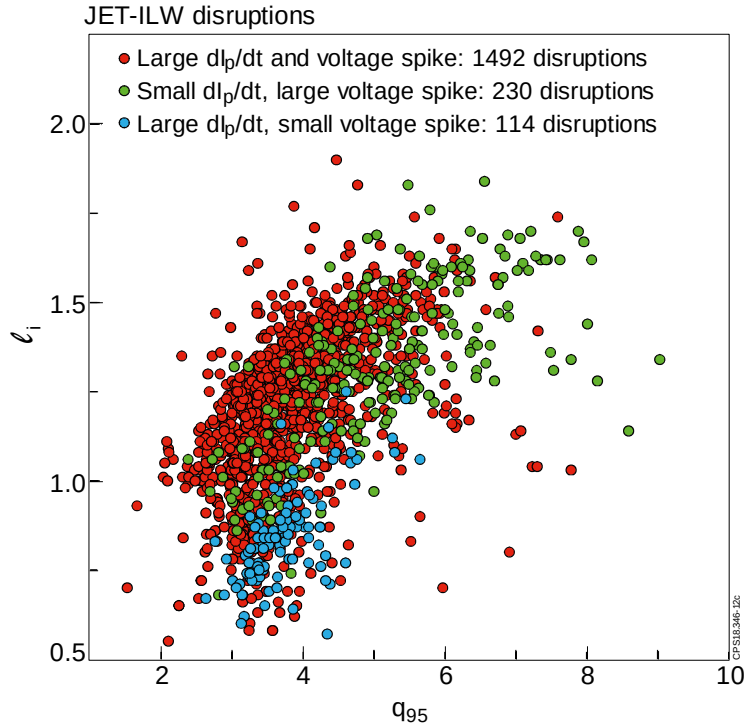

Figure 14. JET-ILW pre-disruptive parameters shown in a l_i-q_{95} stability diagram.

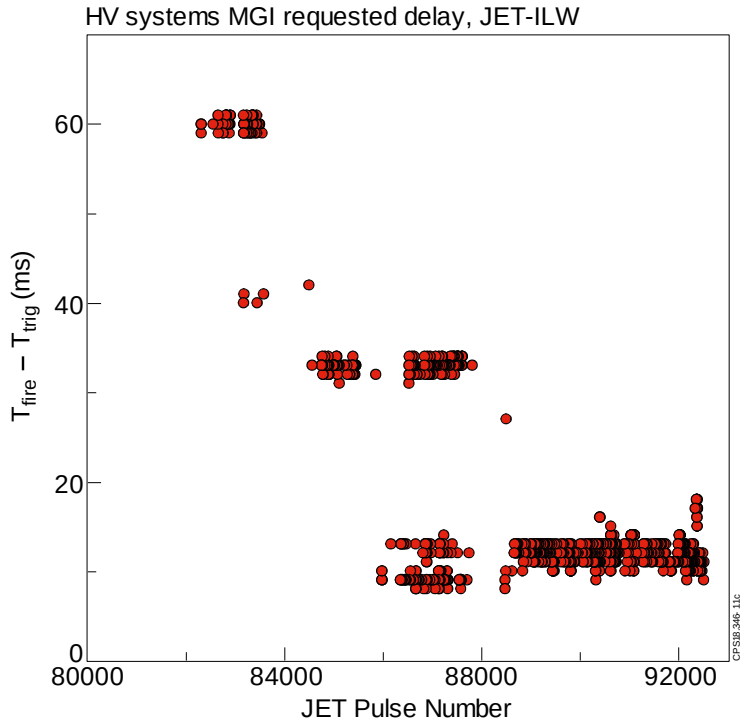

Figure 15. High voltage systems requested MGI delay, which was significantly reduced during of JET-ILW operation.

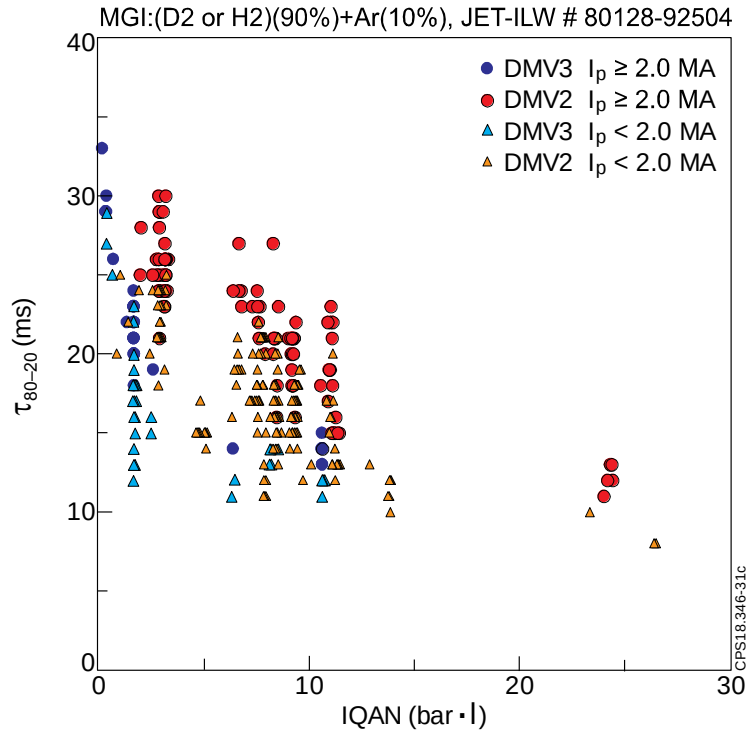

Figure 16. CQ time as a function of amount of injected DMV2 and DMV3 gas. The data presented is for high and low I_p^{dis}.

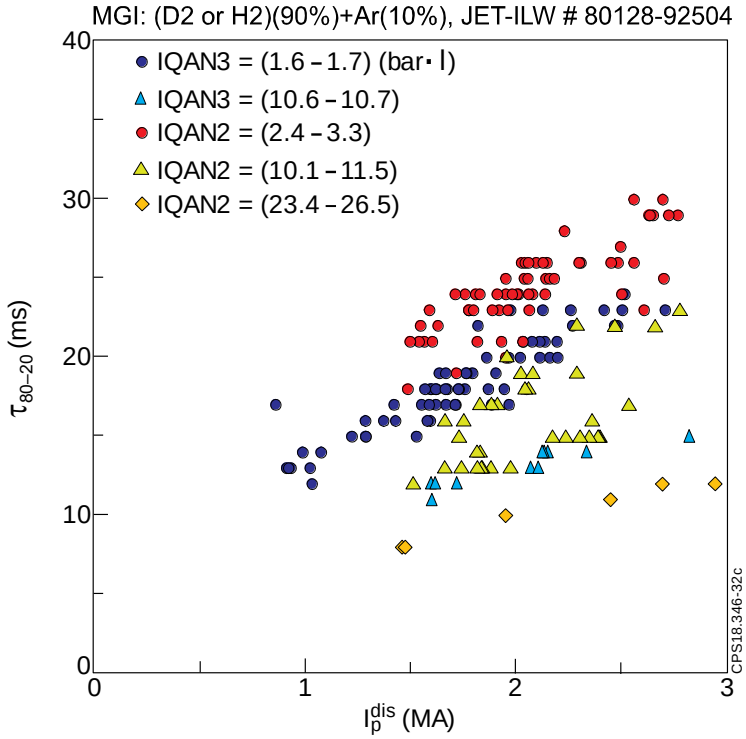

Figure 17. CQ time as a function of pre-disruptive plasma current, I_p^{dis}, for various amount of injected gas IQAN for DMV2 and DMV3 and optimum gas mixture.

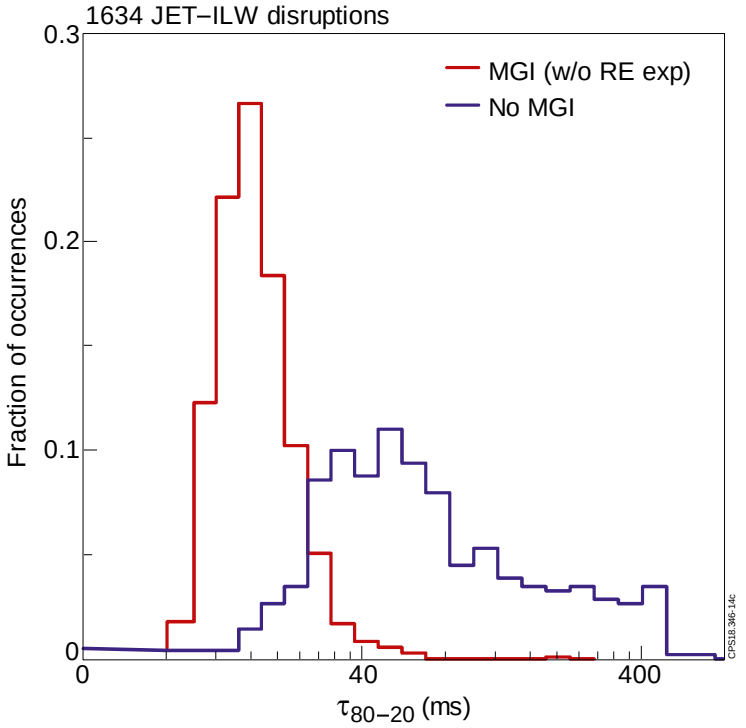

Figure 18. Fraction of distribution occurrences: with and without MGI applied.

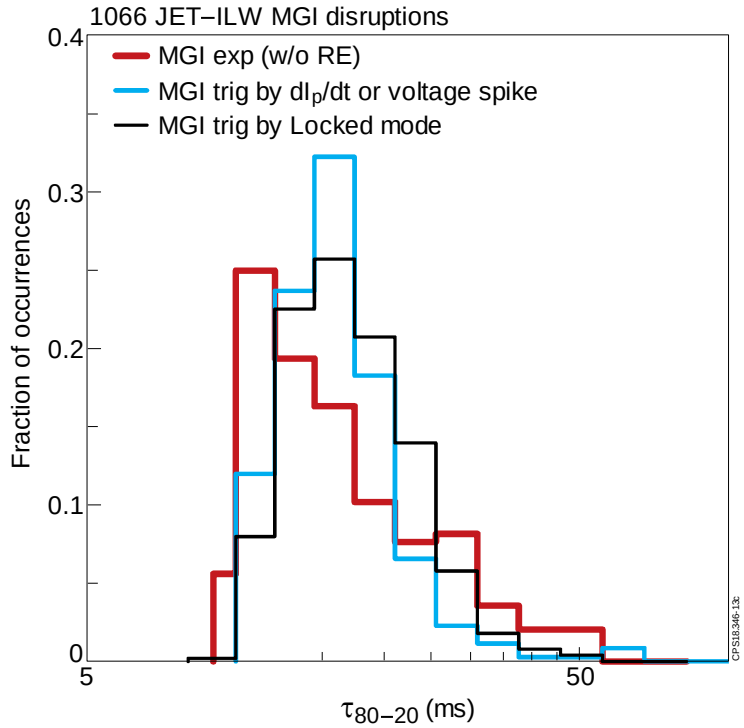

Figure 19. Fraction of distribution occurrences: MGI experiments (when firing in healthy plasma) and when MGI triggered prior or after TQ.

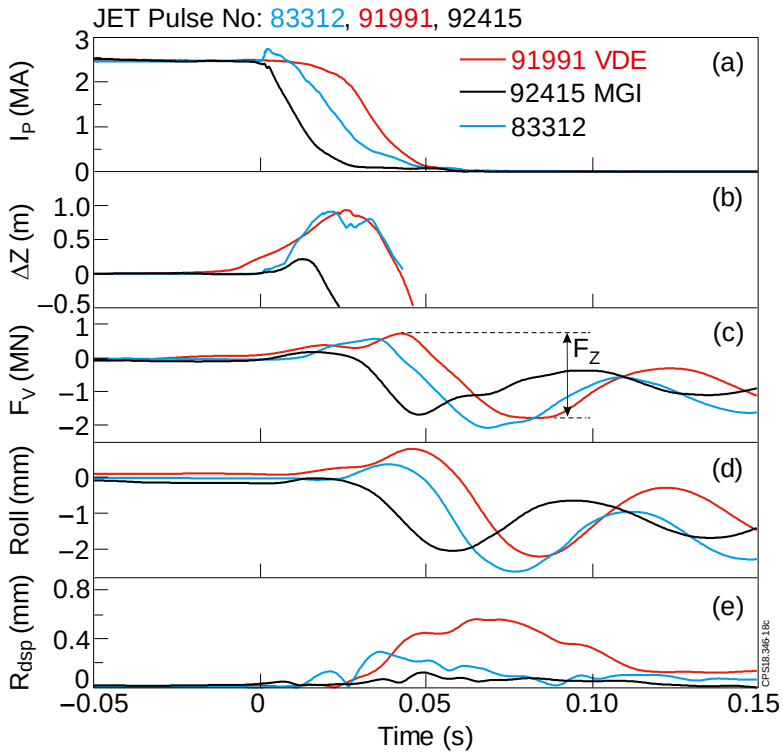

Figure 20. JET vessel reaction on CQ: (a) plasma currents, (b) vertical plasma displacements, (c) vessel vertical (swing) forces, (d) vessel roll, (e) vessel horizontal displacements; #83312 is the centred disruption. The time axis is zeroed to T_{dis}.

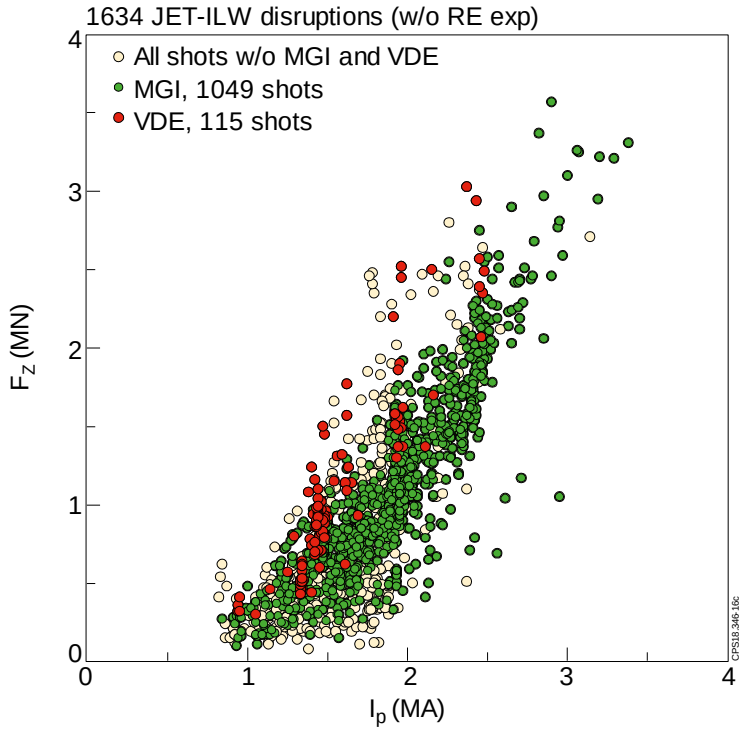

Figure 21. Vessel vertical force vs. pre-disruptive I_p.

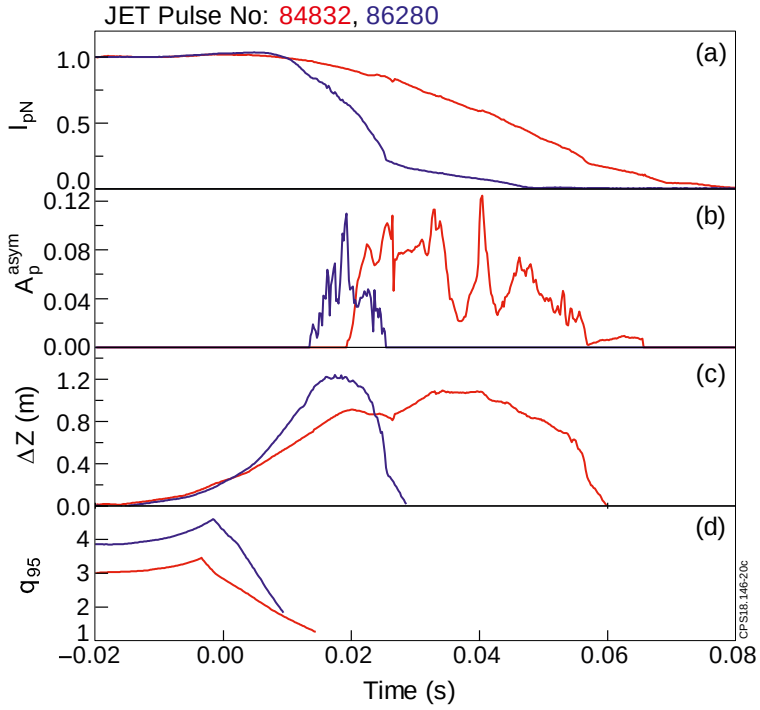

Figure 22. Unmitigated VDEs usually have large I_p asymmetries: (a) normalised plasma currents, (b) I_p asymmetries, (c) plasma vertical displacements, (d) safety factor. The time axis is zeroed to T_{dis}.

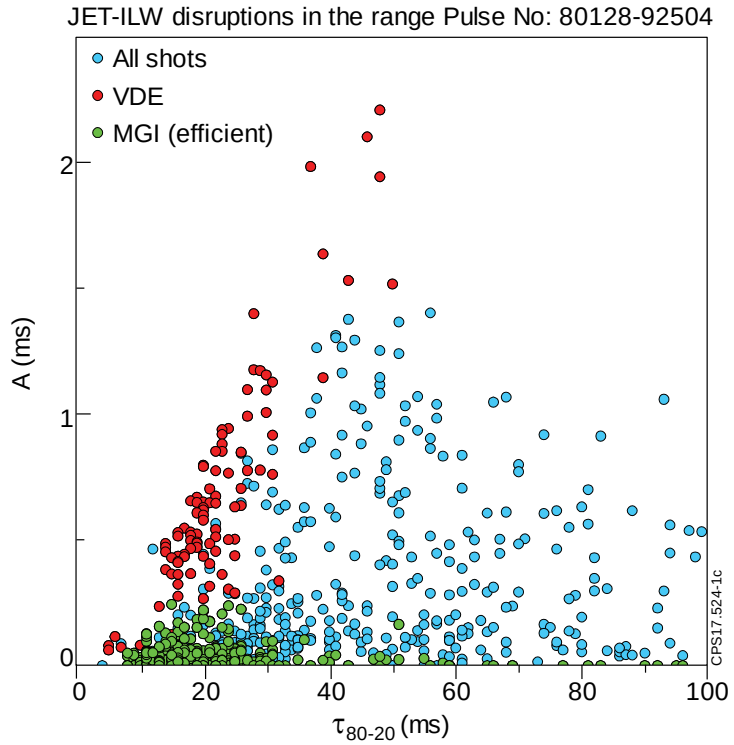

Figure 23. Normalised time integral of plasma current asymmetries vs. CQ time. The MGI efficient pulses are referred to the shots with the optimum pressure and gas mixture, when MGI fired w/o large delay.

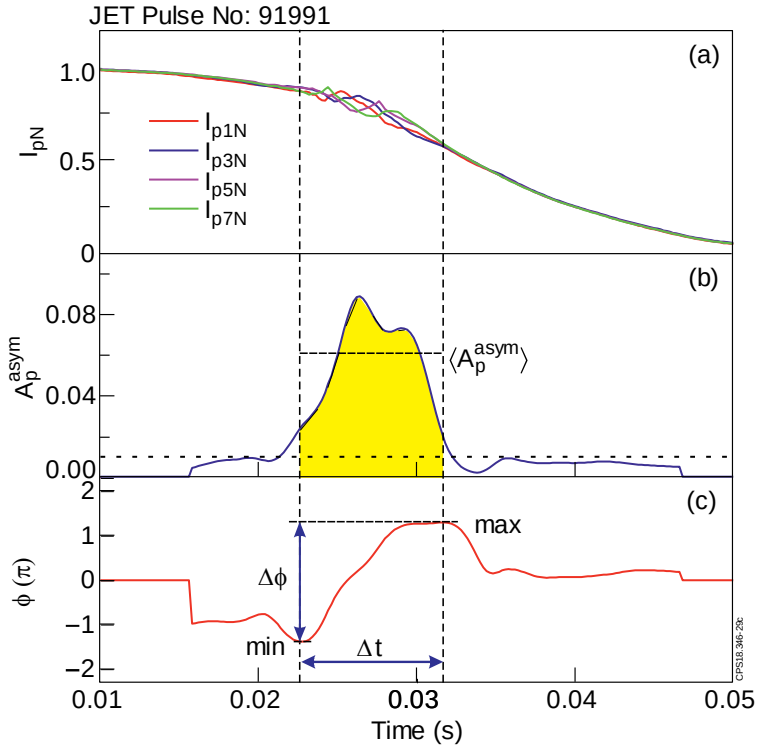

Figure 24. Illustration of calculation of rotational frequency and I_p asymmetry magnitude.

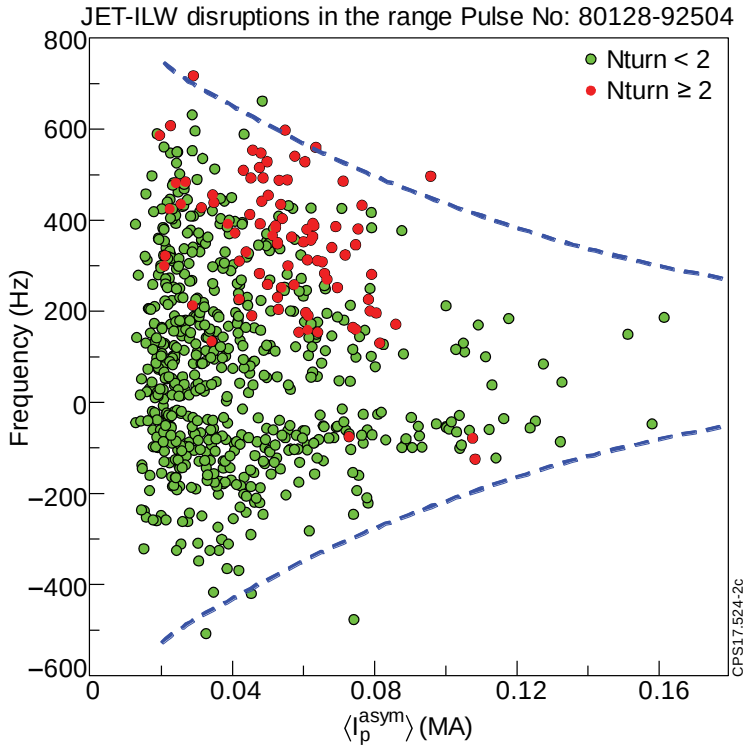

Figure 25. Rotation frequencies vs. I_p asymmetry magnitude.

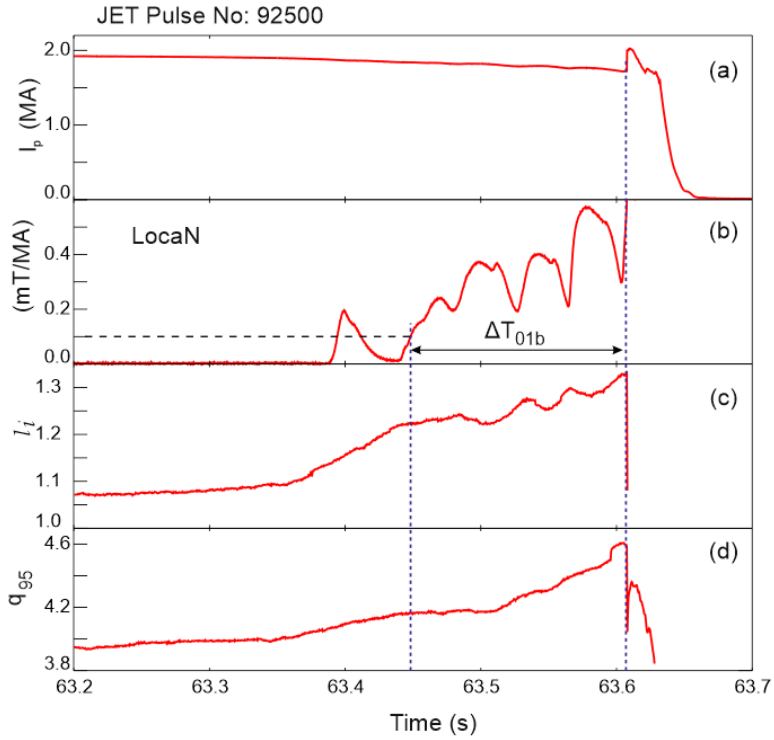

Figure 26. Locked mode precursor: (a) plasma currents, (b) normalised locked mode amplitude; EFIT reconstruction (c) plasma internal inductance, (d) safety factor.

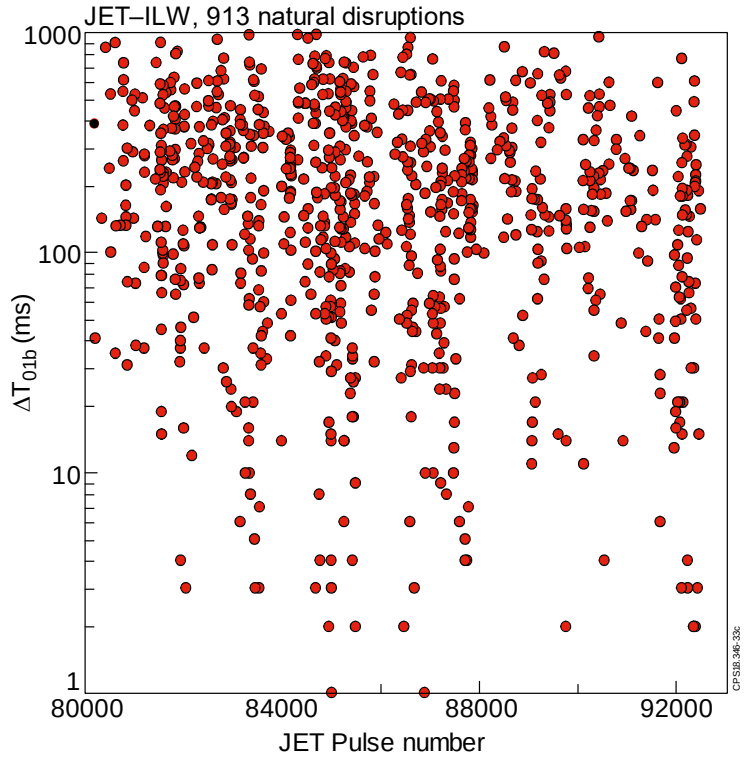

Figure 27. Back time from T_{dis} to when *LocaN* drops below 0.1 mT/MA.